Electronic Supplementary Information (ESI)

Evidence for coexistence of spin-glass and ferrimagnetic phases in $BaFe_{12}O_{19}$ due to basal plane freezing

Keshav Kumar,[a] Shrawan Kumar Mishra,[a] Ivan Baev,[b] Michael Martins,[b] and Dhananjai Pandey*[a]

a. School of Material Science and Technology, Indian Institute of Technology (Banaras Hindu University), Varanasi, India-221005.
b. Universität Hamburg, Institut für Experimentalphysik Luruper Chaussee 149, D-22761 Hamburg, Germany.

1. Experimental

(a) Powder synthesis and crystal growth

Single crystals of $BaFe_{12}O_{19}$ were grown by high-temperature flux method[1]. For this, polycrystalline $BaFe_{12}O_{19}$ was first synthesized by the solid-state reaction method using high purity $BaCO_3$ and Fe_2O_3 (both Sigma Aldrich). For this, the two ingredients were mixed in stoichiometric ratio using mortar pestle for one hour and subsequently using a ball mill for 12 hours in a zirconia jar with zirconia balls in the presence of acetone as the mixing media. This mixture was calcined in an open alumina crucible at 1150^0C for 6 hours. No peak corresponding to impurity phase or unreacted ingredients was detected in the powder diffraction pattern.

The as-calcined powder was mixed with 20wt% Na_2CO_3, which acts as the high-temperature flux, for single crystal growth[1]. This mixture was heated to 1260^0C at a heating rate of 5^0C/min in a closed platinum crucible and then held at 1260^0C for 5 hours for homogenization. The crucible with the molten material was then cooled down to 900^0C at a rate of 4.5^0C per hour and then left to cool down to room temperature in the air as per the protocol given in ref.[1]. Hexagonal platelet-shaped crystals of $BaFe_{12}O_{19}$ were obtained from different parts of the crucible with lateral dimensions of 2 to 4mm and thickness of about 0.8mm. These single crystals were rinsed thoroughly with a warm dilute nitric acid solution to remove the flux from the crystal surfaces.

(b) Characterization techniques

The chemical composition of the crystal was determined using energy dispersive x-ray (EDX) attachment of a scanning electron microscope (SEM, Carl-Zeiss, model no. EVO 18).

The x-ray powder diffraction patterns were obtained using an 18kW rotating anode based high-resolution powder diffractometer (Rigaku, Japan) fitted with a curved crystal monochromator in the diffraction beam, while Laue patterns from the single crystals were recorded using white x-rays from a 12kW x-ray machine.

The temperature-dependent dc magnetization (M(T)) shown in Fig.2 of the main text was measured using a magnetic field of 100 Oe applied parallel (//) and perpendicular (⊥) to the c-axis of the crystals in the temperature range 2 to 200K using a SQUID-based magnetometer (MPMS-3, Quantum Design, USA). The temperature dependence of ZFC and FC M(T), shown in Fig.4(a) of the main text, was measured at 100 Oe field using a physical property measurement system (DynaCool, Quantum Design, USA) PPMS set-up. The frequency-dependent ac-susceptibility $\chi(\omega, T)$ measurements on the same single crystal were carried out at an ac drive field of 3Oe applied perpendicular to the c-axis in the temperature range 2 to 150K using the MPMS-3 set-up. The relaxation of thermoremanent magnetization (TRM) $M_{\perp c}(t)$ was investigated with a magnetic field applied perpendicular to the c-axis below spin glass transition temperature using the PPMS set-up

2. Analysis

(a) Room-temperature crystal structure

The magnetoplumbite structure with $P6_3/mmc$ space group of the as-calcined powder was confirmed by Rietveld technique using x-ray diffraction data. Rietveld refinement was carried out using FULLPROF SUITE[2]. During the refinement, the background was modeled using a six^{th}-order polynomial while the peak shape was modeled using pseudo-Voigt function. The Full-Width at Half-Maxima (FWHM) of the peaks were modeled using the Caglioti equation: $(FWHM)^2 = U\tan^2\theta + V\tan\theta + W$. During the refinement, scale factor, zero displacement, lattice parameters, positional coordinates and thermal parameters were allowed to vary while the occupancy of each ion was fixed at their nominal composition value. The atomic coordinates of

the asymmetric unit of the hexagonal cell with space groups $P6_3/mmc$ of $BaFe_{12}O_{19}$ are given in table S1[3]:

Table S1: Asymmetric unit of the hexagonal phase of $BaFe_{12}O_{19}$ in space groups $P6_3/mmc$.

Atoms	Wyckoff Site	x	y	z
Ba	2d	2/3	1/3	0.25
Fe1	2a	0	0	0
Fe2	2b	0	0	0.25
Fe3	4f1($4f_{iv}$)	1/3	2/3	z
Fe4	4f1($4f_{vi}$)	1/3	2/3	z
Fe5	12k	x	2x	z
O1	4e	0	0	z
O2	4f	1/3	2/3	z
O3	6h	x	2x	0.25
O4	12k	x	2x	z
O5	12k	x	2x	z

The initial input parameters (structural and thermal parameters) were taken from ref[3]. The refinement converged satisfactorily after a few cycles. The observed and calculated profiles obtained after Rietveld refinement are in excellent agreement as can be seen from Fig.S1. This confirms the magnetoplumbite structure of our sample with the $P6_3/mmc$ space group. The structural parameters, thermal parameter, agreement factors, and χ^2 are listed in table S2. The nearest-neighbour interatomic distances, obtained from the refined coordinates using Bond_Str program of FULLPROF SUITE[2], are listed in table S3. The refined lattice parameters and structural parameters given in table S2 are in excellent agreement with those reported in the literature using single-crystal neutron and x-ray diffraction studies[4–6], as can be seen from table S4.

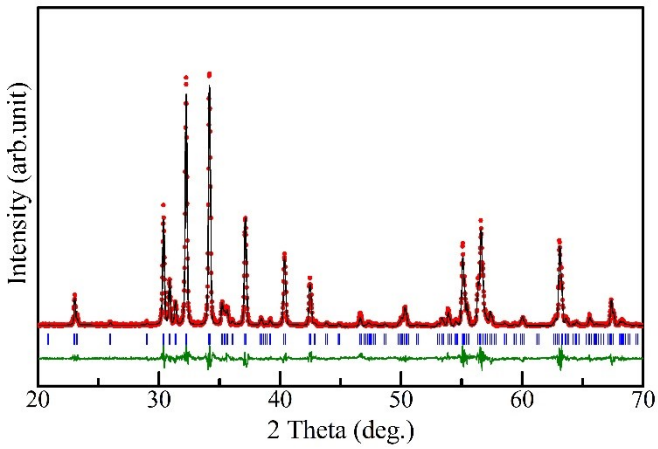

Figure S1: Observed (filled red circles), calculated (continuous black line), and difference (bottom green line) profiles obtained from Rietveld refinement using $P6_3/mmc$ space group for $BaFe_{12}O_{19}$. The vertical bars (blue) represent the Bragg peak positions.

Table S2: Positional coordinates, lattice parameters, and agreement factors obtained by Rietveld refinement of $BaFe_{12}O_{19}$

Atoms/Coordinates	x	y	z	B
Ba	2/3	1/3	0.25	0.8(1)
Fe1	0	0	0	0.7(2)
Fe2	0	0	0.25	0.9(3)
Fe3	1/3	2/3	0.026(3)	0.8(2)
Fe4	1/3	2/3	0.189(3)	0.8(2)
Fe5	0.1731(8)	2x	-0.108(1)	0.0(1)
O1	0	0	0.15(1)	0.5(6)
O2	1/3	2/3	-0.04(1)	0.5(7)
O3	0.19(4)	2x	0.25	0.7(6)
O4	0.15(3)	2x	0.051(5)	0.1(4)
O5	0.49(3)	2x	0.149(6)	0.1(3)
$a = b = 5.890(1)$, $c = 23.186(8)$, $\alpha = \beta = 90$, $\gamma = 120$, $\chi^2 = 3.41$, $R_p = 15.5$, $R_{wp} = 30.0$, $R_{exp} = 16.2$				

Table S3: Interatomic distances (Å) obtained from Rietveld refinement of $BaFe_{12}O_{19}$

Ba polyhedron		**Fe4 octahedron**	
Ba-O3	2.96(3)	Fe4-O3	2.00(3)
Ba-O5	2.90(2)	Fe4-O5	1.92(3)
Fe1 octahedron		**Fe5 octahedron**	
Fe1-O1	3.48(3)	Fe5-O1	2.019(1)
Fe1-O4	2.00(2)	Fe5-O2	2.126(1)
Fe2 trigonal bipyramid		Fe5-O4	2.14(2)
Fe2-O1	2.31(3)	Fe5-O5	3.49(2)
Fe2-O3	1.97(4)	Fe5-O5	1.937(2)
Fe3 tetrahedron		**Important distances**	
Fe3-O2	1.7793)	F5-Fe1	3.066(4)
Fe3-O2	3.442(4)	F5-Fe3	3.499(6)
Fe3-O4	1.878(2)	F5-Fe4	3.498(6)
Fe3-O4	3.46(2)	F5-Fe5	3.059(5)
Fe3-O5	3.229(2)	F5-Fe5	2.831(5)

Table S4: Comparison of our structural parameters with those reported in literature using single-crystal data.

	A	B	C	D
Refined structural parameters	Our results	Single-crystal x-ray diffraction data (main text ref. (4))	Single-crystal neutron diffraction data (ESI ref. (5))	Powder (obtained from crushing the single-crystals) neutron diffraction data (main text ref. (6))
a = b (Å)	5.890(1)	5.8920(3)	5.8948(8)	5.80
c (Å)	23.186(8)	23.183(1)	23.202(3)	23.18
x_{Fe3}	0.026(3)	0.02713(2)	0.02724(9)	0.0271
z_{Fe4}	0.189(3)	0.19030(2)	0.19031(9)	0.1902
z_{Fe5}	0.1731(8)	0.1686(8)	0.1688(3)	0.166(7)
z_{Fe5}	-0.108(1)	-0.10825(1)	-0.10829(4)	-0.108(3)
z_{O1}	0.15(1)	0.15094(13)	0.15033(14)	0.149(7)
x_{O3}	0.19(4)	0.1821(3)	0.1818(7)	0.18(1)
x_{O4}	0.15(3)	0.1564(7)	0.1564(5)	0.16(20)
z_{O4}	0.051(5)	0.05192(8)	0.05204(8)	0.053(9)
z_{O5}	0.149(6)	0.14957(8)	0.14920(7)	0.14(80)

(b) Chemical composition

To check the chemical homogeneity, energy dispersive x-ray (EDX) spectra of the single crystal samples were recorded and a representative spectrum is shown in Fig.S2. This spectrum contains peaks corresponding to Ba, Fe and O only. Analysis of the EDX spectra after averaging

over different regions of one such single crystal is given in table S5. It is evident that the atomic wt.% of Ba and Fe obtained by EDX analysis are close to the nominal compositions. Oxygen was excluded in the analysis as this technique is not sensitive enough for determining the content of low Z elements like O. The results of EDX analysis confirms Ba and Fe stoichiometry of the crystals and absence of any impurity element within the limit of EDX sensitivity.

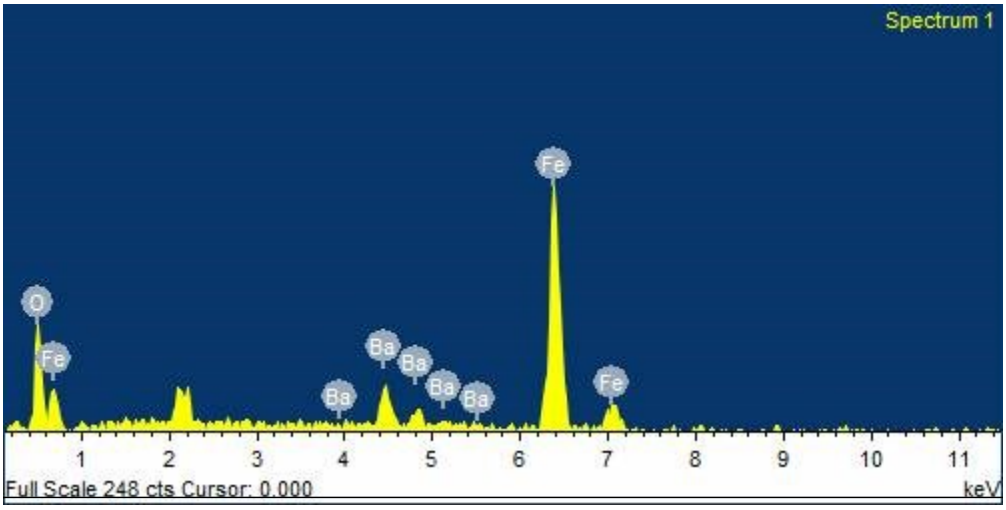

Figure S2: EDX spectra of $BaFe_{12}O_{19}$

Table S5: Average chemical composition of $BaFe_{12}O_{19}$ in atomic wt% obtained from the EDX analysis.

Atoms	Atomic wt.% (As per formula)	Atomic wt.% (From the EDX)
Ba	7.69	7.7 ± 0.7
Fe	92.31	92.3 ± 0.7

(c) Details of ac susceptibility data analysis

For spin-glass systems, relaxation time (τ) follows a power-law behaviour which can be expressed as:

$$\tau=\tau_0((T_f-T_{SG})/T_{SG})^{-zv}, \qquad \text{.....(1)}$$

where τ_0, zv, and T_{SG} have their usual meaning as mentioned in the main text.

Equation (1) can be rewritten as

$$\ln(\tau) = -(zv)\ln((T_f-T_{SG})/T_{SG}) + \ln(\tau_0), \qquad \text{.....(2)}$$

which is the equation of a straight line

$$y = mx + c, \qquad \text{……..(3)}$$

with $y = \ln(\tau)$, $c = \ln(\tau_0)$, $m = -z\nu$, and $x = \ln((T_f - T_{SG})/T_{SG})$. Since there are three unknowns in Equation(2) ($z\nu$, τ_0, and T_{SG}) whereas only two unknowns can be determined using least-squares straight-line fit as per Equation(3), we followed the procedure given in ref.[7]. In this approach, one choose different values of T_{SG} and carries out least-squares fit for $\ln(\tau)$ vs $\ln((T_f - T_{SG})/T_{SG})$. The variance ($\sigma$) obtained for each value of T_{SG} by least-squares fit is plotted in Fig.S3 as a function of T_{SG}. It is evident from Fig.S3 that σ shows a minimum at T_{SG} =46.035 with a step of 0.005 (i.e., at which T_{SG} was chosen around the minimum value of σ). In this way, we obtained the best fit value of T_{SG} (46.035±0.005). Using this best fit value of T_{SG}, we have plotted $\ln(\tau)$ vs $\ln((T_f - T_{SG})/T_{SG})$ in Fig.4(c) of the main text. The least-squares best fit parameters so obtained are $z\nu$ = (0.50±0.02) and τ_0 =(8.2± 0.8) x10^{-5}s.

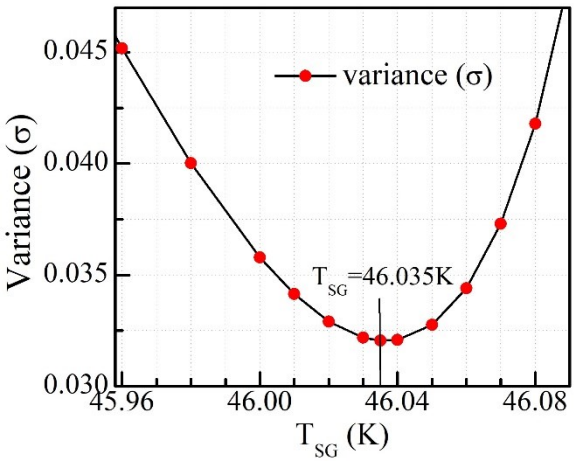

Figure S3: Variation of variance (σ) as a function of spin-glass transition temperature T_{SG}.

Electronic supplementary information references

1 V. V. Atuchin, D. A. Vinnik, T. A. Gavrilova, S. A. Gudkova, L. I. Isaenko, X. Jiang, L. D. Pokrovsky, I. P. Prosvirin, L. S. Mashkovtseva and Z. Lin, *Journal of Physical Chemistry C*, 2016, **120**, 5114–5123.

2 J. Rodríguez-Carvajal, FULLPROF 2017, http://www.ill.eu/sites/fullprof.

3 W. D. Townes, J. H. Fang and A. J. Perrotta, *Z. Kristallogr.*, 1967, **125**, 437–449.

4 X. Obradors, A. Collomb, M. Pernet, D. Samaras and J. C. Joubert, *Journal of Solid State Chemistry*, 1985, **56**, 171–181.

5 H. B. Cao, Z. Y. Zhao, M. Lee, E. S. Choi, M. A. McGuire, B. C. Sales, H. D. Zhou, J. Q. Yan and D. G. Mandrus, *APL Materials*, 2015, **3**, 062512.

6 O. P. Aleshko-Ozhevskii, M. K. Faek and I. I. Yamzin, *Soviet Physics-Crystallography*, 1969, **14**, 367–369.

7 E. Courtens, *Physical Review Letters*, 1984, **52**, 69–72.